Physics of the Earth and Planetary Interiors 246 (2015) 52–71

Contents lists available at ScienceDirect

Physics of the Earth and Planetary Interiors

journal homepage: www.elsevier.com/locate/pepi

Invited review

Rotating convective turbulence in Earth and planetary cores

J.M. Aurnou [a,b,*], M.A. Calkins [c], J.S. Cheng [b], K. Julien [c], E.M. King [d], D. Nieves [c], K.M. Soderlund [e], S. Stellmach [f]

[a] Institut de Recherche sur les Phénomène Hors Equilibre, Marseille, France
[b] Department of Earth, Planetary & Space Sciences, University of California, Los Angeles, USA
[c] Department of Applied Mathematics, University of Colorado, Boulder, USA
[d] US Global Development Lab, US Agency for International Development, Washington, DC, USA
[e] Institute for Geophysics, University of Texas at Austin, USA
[f] Institut für Geophysik, Westfälische Wilhelms-Universität, Münster, Germany

ARTICLE INFO

Article history:
Received 14 December 2014
Received in revised form 7 June 2015
Accepted 10 July 2015
Available online 23 July 2015

Keywords:
Core dynamics
Convection
Turbulence
Dynamo theory

ABSTRACT

An accurate description of turbulent core convection is necessary in order to build robust models of planetary core processes. Towards this end, we focus here on the physics of rapidly rotating convection. In particular, we present a closely coupled suite of advanced asymptotically-reduced theoretical models, efficient Cartesian direct numerical simulations (DNS) and laboratory experiments. Good convergence is demonstrated between these three approaches, showing that a comprehensive understanding of the dynamics appears to be within reach in our simplified rotating convection system. The goal of this paper is to review these findings, and to discuss their possible implications for planetary cores dynamics.

Contents

1. Introduction . . . 53
2. Methods of studying rapidly-rotating convection . . . 57
 2.1. Laboratory experiments . . . 58
 2.2. Direct numerical simulations . . . 58
 2.3. Asymptotically reduced models . . . 58
3. Rapidly-rotating convection results . . . 60
 3.1. Flow morphologies . . . 60
 3.2. Heat transfer . . . 63
 3.3. Large-scale coherent structures . . . 66
4. Extrapolations and predictions . . . 66
 4.1. Geostrophic turbulent convection . . . 66
  4.1.1. Low Prandtl number considerations . . . 67
 4.2. Large-scale vortices . . . 68
 4.3. Magnetohydrodynamic considerations . . . 68
5. Summary . . . 68
 Acknowledgements . . . 69
 References . . . 69

* Corresponding author at: Department of Earth, Planetary & Space Sciences, UCLA, USA.
E-mail address: jona@epss.ucla.edu (J.M. Aurnou).

http://dx.doi.org/10.1016/j.pepi.2015.07.001
0031-9201/

1. Introduction

Earth's global-scale magnetic field is generated deep inside our planet, within the iron-rich core. Flows of molten metal in the liquid outer core, which are likely driven by thermo-chemical buoyancy forces, continually regenerate the geomagnetic field, creating a self-sustaining planetary dynamo. Fig. 1a shows the radial component of the geomagnetic field in 2000 A.D. plotted on the core-mantle boundary (CMB) (Jackson, 2003). In this image, the field is spatially-resolved up to spherical harmonic degree 13; higher order components are masked by the magnetization of Earth's crust (e.g., Fig. 3 in Roberts and King, 2013). The magnetic field is dominated by its axial dipolar component, with magnetic flux predominantly emerging from the southern hemisphere and returning back through the CMB in the northern hemisphere. Most of the axial dipole's energy is contained in four strong high latitude flux patches, two in the northern hemisphere and two in the southern hemisphere (e.g., Olson and Amit, 2006). These flux patches are located in the vicinity of the tangent cylinder, the imaginary axial cylinder shown schematically in Fig. 1d that circumscribes the solid inner core's equator. Magnetic flux patches exist in the vicinity of the magnetic equator as well. These equatorial flux patches also contain significant magnetic energy (Jackson, 2003). Due to their low latitude placement, they contribute principally to the higher, non-dipolar axial components of the geomagnetic field.

At present, numerical simulations form the primary tool for studying dynamo processes on Earth and the other planets (e.g., Stanley and Glatzmaier, 2010). Dynamo action develops in these simulations, primarily driven by axially-aligned columnar flows that qualitatively resemble non-magnetic rotating convection (e.g., Kageyama and Sato, 1997; Olson et al., 1999; Ishihara and Kida, 2002; Aubert et al., 2008; Soderlund et al., 2012; Sreenivasan et al., 2014). For example, Fig. 1b shows a snapshot of the radial component of the magnetic field on the outer boundary of a spherical shell dynamo simulation from the study of Soderlund et al. (2012), with resolution up to spherical harmonic degree 64. In this image, strong magnetic flux patches are evident at higher latitudes near where the tangent cylinder intersects the outer boundary. Further, strong flux patches are generated with a high degree of symmetry across the geographic equator. (For detailed descriptions of magnetic induction processes in planetary dynamos and numerical dynamo models, we refer to a number of recent review articles: Sreenivasan (2010), Jones (2011), Roberts and King (2013).)

The magnetic field in Fig. 1b is generated by simultaneously solving the evolution equations of convection-driven magnetohydrodynamic induction in a spherical shell with outer boundary r_o and inner boundary r_i (e.g., Glatzmaier, 2013):

$$\partial_t \mathbf{u} + (\mathbf{u}\cdot\nabla)\mathbf{u} = -\nabla p + (Ra\,Pr^{-1})\Theta(\vec{r}/r_o) + \nabla^2\mathbf{u} - E^{-1}\hat{z}\times\mathbf{u} + (E\,Pm)^{-1}(\nabla\times\mathbf{B})\times\mathbf{B}, \quad (1)$$

$$\partial_t \Theta + (\mathbf{u}\cdot\nabla)\Theta = Pr^{-1}\nabla^2\Theta, \quad (2)$$

$$\partial_t \mathbf{B} + (\mathbf{u}\cdot\nabla)\mathbf{B} = (\mathbf{B}\cdot\nabla)\mathbf{u} + Pm^{-1}\nabla^2\mathbf{B}, \quad (3)$$

subject to the solenoidal conditions $\nabla\cdot\mathbf{u} = 0$ and $\nabla\cdot\mathbf{B} = 0$ for the velocity and magnetic fields, $\mathbf{u}$ and $\mathbf{B}$, respectively. The first equation describes the conservation of momentum in a rotating

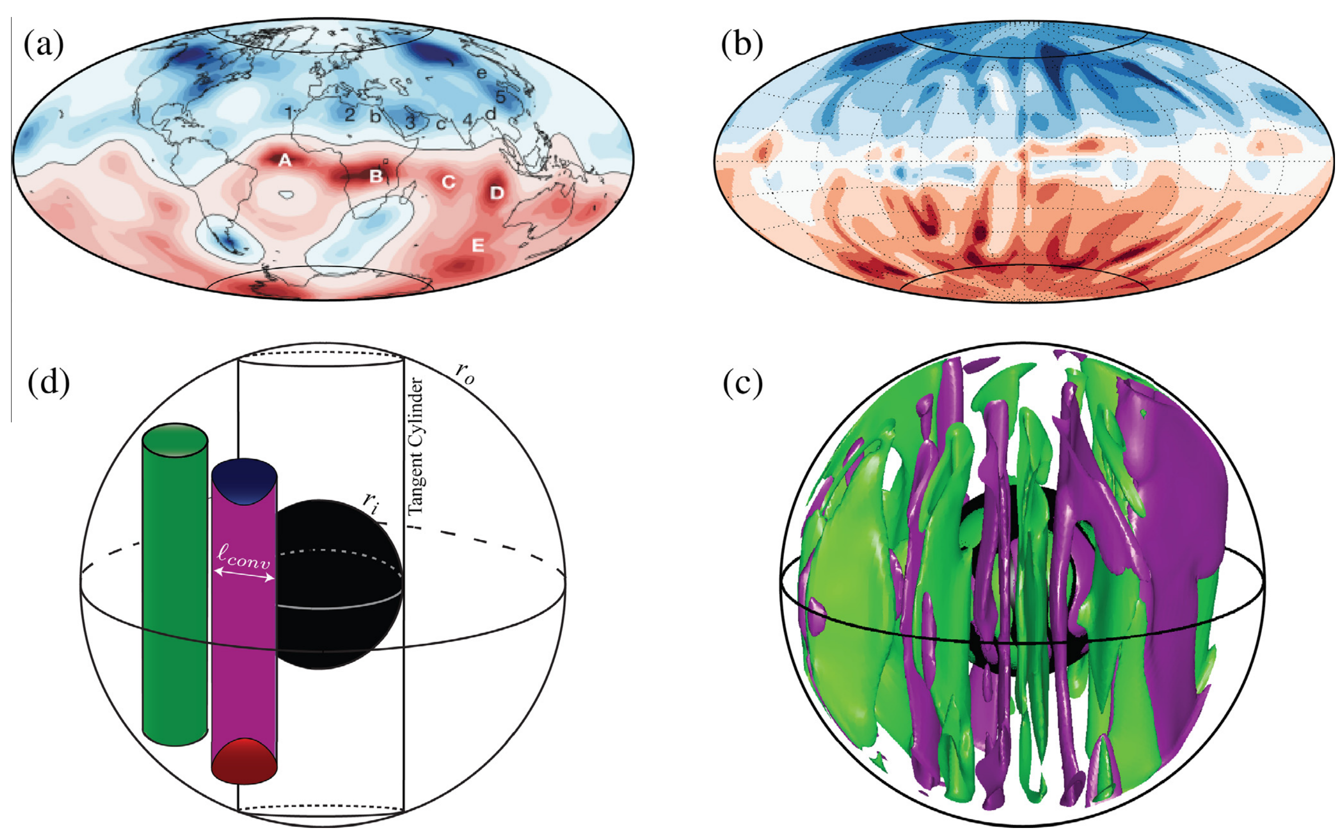

Fig. 1. (a) Radial magnetic field, B_r, on Earth's core-mantle boundary (CMB), adapted from Jackson (2003). Red (blue) denotes magnetic field parallel (antiparallel) to the radial outward normal vector. (b) Outer boundary B_r from a numerical simulation by Soderlund et al. (2012); $E = 10^{-4}; Pr = 1; Pm = 2, Ra = 1.42\times10^6 = 1.9Ra_{crit}$, and radius ratio $\chi = r_i/r_o = 0.4$. The intersection of the tangent cylinder with r_o is denoted by the solid black lines at $\cos^{-1}(\chi) = \pm66.4^\circ$ latitude. (c) Axial vorticity, $\zeta = \hat{z}\cdot(\nabla\times\mathbf{u})$, rendered from the same $Ra = 1.9Ra_{crit}$ case. Purple (green) denotes fluid vorticity aligned parallel (antiparallel) to the system's rotation axis. (d) Schematic of laminar axial convection columns of width ℓ_{conv}, with associated large-scale outer boundary magnetic flux patches shown at the ends of the cyclonic columnar structure ($\zeta > 0$, purple).